Chapter 9

Laser Ablation in Liquid: An Unconventional, Fast, Clean and Straightforward Technique for Material Preparation

Walter Mendes de Azevedo ,
Sérgio de Lemos Campello , Diego Leite da Cunha ,
Leonardo Tadeu Boaes de Mendonça and
Ohanna Maria Menezes Madeiro da Costa

Additional information is available at the end of the chapter

http://dx.doi.org/10.5772/66245

Abstract

The laser ablation in liquid environment (LALE) technique is a straightforward experimental technique with few controllable parameters, capable to provide extreme pressure and temperature conditions during target ablation without the need for dedicated systems to provide those variables. Additionally, we can state that LALE can be considered a low-cost experimental technique, with few steps and a clean synthesis method, by which a wide variety of materials can be synthesized with high yield. The majority of studies published in the literature using this technique seem to be limited only to the synthesis of metal nanoparticles, metal oxides, nitrates and semiconducting. However, in order to extend the synthesis potential of this technique, in this chapter we are going to demonstrate that with the appropriate choice of reactants, solvent, target materials and the solid-liquid interface interactions we will be able to prepare more complex molecules such as carbonate compound $Pb_3(CO_3)_2(OH)_2$, metal-organic frameworks (MOFs), luminescent metal-organic frameworks (LMOFs), highly dispersed CdS quantum dots and magnetic materials. Also for each material synthesized, we are going to propose a mechanism to explain its preparation using the LALE technique.

Keywords: laser ablation in liquid, nonconventional synthesis, materials preparation, complex compounds, inorganic compound

1. Introduction

Searching the literature we can observe that there is a huge amount of techniques that can be used for material preparation. As a matter of fact, for each group of materials there is a specific route more suitable to be used. An interesting conclusion we can make is the fact that unusual properties obtained in a specific material is sometimes related to the selected preparation method. To be more specific, not only the method used but also the solvent, the concentration, the manner, or the sequence in which the reaction components are mixed make these characteristics more pronounced when we are taking into consideration the preparation of nanomaterials.

On the other hand, among several methods developed in the last decade for material preparation, it can be observed that one stands apart: the pulsed laser ablation technique (PLA). The reason seems to be the high potential presented by the laser-based material processing for the thin solid film preparation, nanocrystal growth, surface cleaning and microelectronic device fabrication [1–5]. The pulsed laser ablation of solid materials was initially carried out in a conventionally evacuated deposition chamber and the majority of the results have focused on pulsed laser deposition (PLD) of solid targets in vacuum and in a diluted gaseous ambient [6, 7].

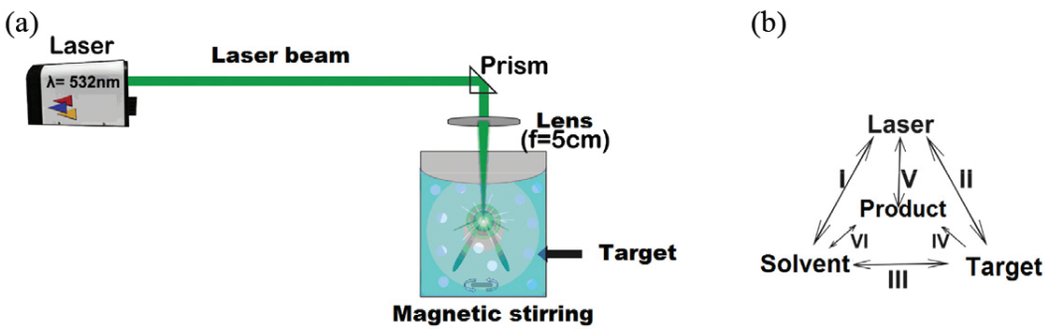

Figure 1. (a) Experimental set up for the LALE experiments (b) interaction diagram.

Moreover, a slight modification of the PLD technique for materials preparation is the laser ablation in liquid environment (LALE). This technique has been extensively used at the beginning for the preparation of colloidal solution of metallic nanoparticles and subsequently as a successful technique for the fabrication of nanostructured metals oxide, nitrate and other materials of various compositions, morphologies and phases [8, 9]. Additionally, this technique nowadays can be considered a chemically clean and one-pot synthetic route by which a variety of functionalized new nanostructures can be prepared with a high yield of the final product without any by-products and, mostly, there is no need for further purification.

Compared with others techniques, LALE can be considered as a low cost experimental technique, which presents few controllable parameters and provides extreme experimental conditions of high temperature and pressure that favors the formation of unusual metastable phases. The technique consists of the interaction of a high-intense Laser pulse with a solid

http://dx.doi.org/10.5772/66245

target immersed in a liquid solution as shown in **Figure 1(a)**. In this case, both the ablation of the target material and the interaction of the laser beam with the solvent (**Figure 1b**) occur simultaneously. As a consequence, the plasma plume formed by the target ablation expands and is confined by the liquid. Some works indicated that the density of the ablated species is of the order of 10^{22}–10^{23} cm^3, the temperature could reach 4000–5000 K and the pressure is of the order of 10 GPa inside the plasma plume generated by the ablation in liquid [8]. According to Ogata and coworkers [10], interesting chemical reactions could take place at the interface between the plasma plume and the liquid, allowing the synthesis of a new chemical compound.

Although this technique has proved to be an excellent route for material preparation, this methodology has been used mainly to obtain metal oxide, metals colloids, semiconductor and nitrites [11–17]. Therefore, it will be presented, in detail, the synthesis of five chemical compounds prepared by the LALE technique that had been prepared at the Solid State Laboratory of Federal University of Pernambuco in order to demonstrate the versatility of the laser ablation technique and also to convince the scientific community that this is a very powerful tool for the preparation of complex materials.

2. Experimental

Figure 1 shows the experimental set up used for all compounds preparation. For the target ablation, a second harmonic of a pulsed Nd:YAG laser (Spectra-Physics Quanta-Ray GCR-170 or a Quantel, model Brilliant B) is used, operating at 10 Hz with 8 ns of pulse width, with the beam focused on the target with a spot size of about 1 mm in diameter using a lens with a focal length of 50 mm. The synthesis processes differ from each other only on the Laser fluency used, ablation time, kind or type of target, solvent used and the proposed mechanism that explains its formation.

2.1. Synthesis of $Pb_3(CO_3)_2(OH)_2$

For the synthesis of the carbonate compound $Pb_3(CO_3)_2(OH)_2$, a target of solid Pb metal (99.5%, from America Elements) was used and ablated for 10 minutes with a pulsed Nd:YAG laser as shown in **Figure 1**. Finally, the products were centrifuged and collected. The solutions obtained, including sediments, were dropped and dried on glass substrates for sample characterization. For the purpose of comparing the results, three different laser fluencies on the solid target were used: 0.5, 1.0 and 2.0 J/cm^2 and in order to establish the mechanism for sample preparation, the ablation reaction was performed in methanol (Merck PA), ethanol (Kinetics PA), 1-propanol (Merck PA) and 1-butanol (Merck PA) [17, 18].

2.2. Synthesis of CdS quantum dots

In this case, the synthesis of the nanostructured CdS quantum dots was performed using a metal cadmium foil, which is 0.5 mm thick (99.99%) from Aldrich Company as a target for the Cd ion source production and thiosulfate and thioglycerol from Merck company as a sulfur source. The cadmium metal foil was washed with a mixture of H_2O:HNO_3 1:1 (v/v) to remove

the oxide layer, followed by distilled water and acetone washing under ultrasound bath for 5 min.

The Cd foil was immersed in a Beaker (50 ml) filled with aqueous solution of thiosulfate (5, 7, 9, 12 and 15 mmols) and thioglycerol (5 mmols) and ablated for 5 min with the second harmonic order light pulse of a Nd:YAG laser. Soon after the ablation starts, the solution changes its color from transparent to yellow as an indicator that the reaction is taking place. Finally, the products were centrifuged and washed several times with acetone and the material was collected for characterization [19].

2.3. Synthesis of magnetic iron compounds

For the synthesis of magnetic nano– and micro–iron oxide particles, the solid iron targets were ablated immersed in an aqueous solution of basic pH. As a result of the iron ablation, we observed the formation of ions ferrate (VI), α-iron and the unusual form of iron oxides FeO. The aim of this study is to evaluate how the material contained in the plasma plume formed by the laser ablation of an iron target evolves into a medium of high pH and chemically reacts with the solution to form iron oxides. We also examined how the fluency of laser pulses applied to solid iron target surface influences the preparation process.

For this experiment, we used Fe plates that were chemically cleaned, washed with water and then subjected to ultrasonic bath in ethanol for 5 min. The ambient liquid used was a solution with a concentration of 1 molar sodium hydroxide in distilled water and measurements indicated that the pH of the solution was 14. The ALAL was performed with three laser beam fluency values, the materials prepared under these conditions were designated as Type1, Type2 and Type3 and **Table 1** shows the synthesis parameters used for the preparation of these samples. All experiments were conducted at a temperature of 293 K and pressure of 1 atm. To minimize the number of variables in the preparation process, the same values for repetition rate of the laser pulses and the height of the liquid layer on the solid target (10 mm) were used, both for the volume to the liquid environment and for the laser ablation time at which the target has been subjected.

Sample	Solid target	Liquid environment	Fluency (J/cm^2)	Frequency (Hz)	Ablation time (min)
1	Iron (bulk)	20 ml of NaOH 1.0 M	0.5	10	10
2	Iron (bulk)	20 ml of NaOH 1.0 M	2.0	10	10
3	Iron (bulk)	20 ml of NaOH 1.0 M	4.0	10	10

Table 1. Experimental parameters for ALAL of iron plates.

2.4. Synthesis of $Cu_3(BTC)_2(H_2O)_3$

For the synthesis of the $Cu_3(BTC)_2$ MOF, a Cu powder metal (99.5%) was used as a target for the ablation dispersed in a solution of a DMF/H_2O (1:1) containing the organic linker benzene 1,3,5, benzene tricarboxilic acid and $NaNO_3$ as a hydroxyl radicals (•OH) precursor. The target

http://dx.doi.org/10.5772/66245

was ablated for 60 min under magnet stirring with the second harmonic of a pulsed Nd:YAG laser. Soon after the ablation starts, the solution changes its color and a blue precipitate occurs. Finally, the products were centrifuged and collected for sample characterization [20].

2.5. Synthesis of $Eu(TMA)(H_2O)_4$

For the synthesis of the microstructured luminescent MOF $Eu(TMA)(H_2O)_4$, instead of using metal or metal powder as a target, europium oxide powder (Eu_2O_3) (99.99%, Sigma Aldrich) was used as a target. In this case, the powder was dispersed in a solution of DMF/H_2O (1:1), containing the organic linker Trimesic acid (TMA) and sodium nitrate ($NaNO_3$) under a magnetic stirring. As it is shown in **Figure 1**, the target was irradiated for 60 min with the second harmonic (λ = 532 nm) of a pulsed Nd:YAG laser. It is interesting to notice that as the ablation starts, the solution changes its optical characteristic, with the initial transparent solution becoming milk-like white as the reaction continues and finally a white precipitate occurs. In order to characterize the materials, the products were centrifuged, washed with hot water several times and dried under vacuum. Sample characterization allows us to conclude that the reaction yield is of the order of 70%. Compared with the literature results for different synthesis method we can conclude that it is a good yield [21–23].

3. Material characterization

Spectroscopic characterization in the UV-visible and infrared region was performed with an Ocean Optics model 2000 spectrophotometer and with a FTIR/FT-NIR Spectrometer model Spectrum 400 Perkin Elmer, respectively, while room temperature photoluminescence (PL) was measured in Ocean optics model QE65000 spectrophotometer with the sample been exited with a N_2 laser or in a Horiba Jobin Yvon spectrofluorometer model Fluorolog-3 FL3-22 using a 450-W xenon short-arc lamp light as the excitation source. The luminescence quantum yields measurements were recorded with a Horiba Jobin Yvon spectrofluorometer using an integrating sphere model F-3018.

The particle morphology and structure was characterized by transmission electron microscope (TEM) and X-ray diffraction measurement, using a Tecnai 20 transmission electron microscope operating with an accelerating voltage of 200 KV and a Rigaku diffractometer model DMAX 2400, using Cu K_ radiation (λ = 0.154 nm) at a scanning speed of 0.1° s^{-1} in the range of 2θ = 10–60° with a step 0.02°, respectively. The sample for the TEM measurements was diluted and dropped onto a carbon-covered 200-mesh copper grid followed by natural evaporation of the solvent.

4. Results and discussion

The first example of a compound synthesized by LALE technique shown in this chapter is the synthesis of hydrocerussite $Pb_3(CO_3)_2(OH)_2$, a quite rare mineral in nature that is found in soil

only in small quantities. It consists of basic lead carbonate with a trigonal crystalline structure [24]. Although it is rare in nature, it was extensively synthesized and used not only as a cosmetic or in religious and medical practices [25] from Ancient Egypt to the Greco-Roman period [26] but also as a white pigment in easel painting [27] from the Renaissance to the end of the nineteenth century. More recently, it has been playing a significant role in geology, in environmental issues [28, 29], applied as a polymer stabilizer [30] and has been extensively investigated in the lead acid battery industry because its presence in battery plates increases the resistivity of the electrolyte [31].

The ablation of a Pb target in methanol or ethanol results in a whitish powder precipitation while a grayish color solution was obtained when 1-propanol or 1-butanol was used. The mechanism proposed to explain the whitish precipitated material is demonstrated in the scheme below, in which the ablation of the Pb target in a solution produces Pb atoms, ions and Pb particles that become dispersed in the liquid environment and subsequently interact with absorbed O_2 to form the lead oxide PbO.

The decomposition of methanol into CO_2 and H_2O is catalyzed by the ablated metal that remains in solution [32–34]. The remaining CO_2 reacts with PbO to form the hydrocerussite compound.

$$\mathrm{Pb_{(solid)}} + h\nu + \mathrm{O_2} \rightarrow n\mathrm{Pb} + \mathrm{Pb}^{+m} + \mathrm{PbO} \tag{1}$$

$$\mathrm{CH_3OH} + \mathrm{O_2} \xrightarrow{hn + n\mathrm{Pb}^0} \mathrm{CO_2} + \mathrm{H_2} + \mathrm{H_2O} \tag{2}$$

$$3\mathrm{PbO} + \mathrm{CO_2} + \mathrm{H_2} \rightarrow \mathrm{Pb_3}\left(\mathrm{CO_3}\right)\left(\mathrm{OH}\right)_2 \tag{3}$$

In order to prove the efficacy of the mechanism proposed in **Figure 2**, we present the X-ray diffraction analysis of the samples prepared in methanol, ethanol 1-propanol and 1-butanol. For the samples prepared in methanol and ethanol the diffraction peaks correspond to the crystalline planes of the trigonal crystalline structure of the hydrocerussite reported on JCPDS card 130131. While for the Pb target ablated in 1-propanol and 1-butanol it is observed that diffraction peaks refer to the hydrocerussite and the crystalline planes of the cubic FCC of metallic phase lead to a structure in agreement with the reported on JCPDS card 040686. It is interesting to notice that the metal became the major phase for the Pb target ablated in 1-butanol.

In conclusion, we may say that if we carefully choose the solvent, we are able to decide which material will be synthesized. Hydrocerussite is obtained when the Pb target is ablated in ethanol and methanol solution whereas hydrocerussite and Pb metal particles are obtained from the solvent 1-propanol and 1-butanol and the metallic phase is more abundant in 1-butanol.

http://dx.doi.org/10.5772/66245

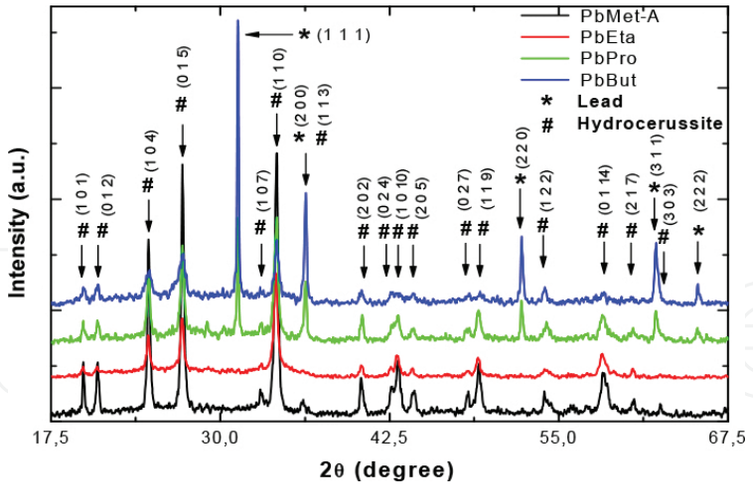

Figure 2. XRD patterns recorded for the samples PbMet-A, PbEtha, PbPro and PbBut. The crystalline phases and main crystalline planes associated with each phase are also shown.

As a matter of fact, several metal nanoparticles such as cobalt, nickel, silver, copper, palladium and semiconductor quantum dots (QDots) [35–39] have been obtained using the reducing power of alcohols with large carbon chains.

Figure 3 shows the SEM characterization for the sample prepared in methanol and it is observed that a hexagonal structure was obtained with average widths of 1.0 ± 0.3 μm and an average thickness of 80 ± 20 nm. This result is similar to the morphology results found in the literature for hydrocerussite [24, 40].

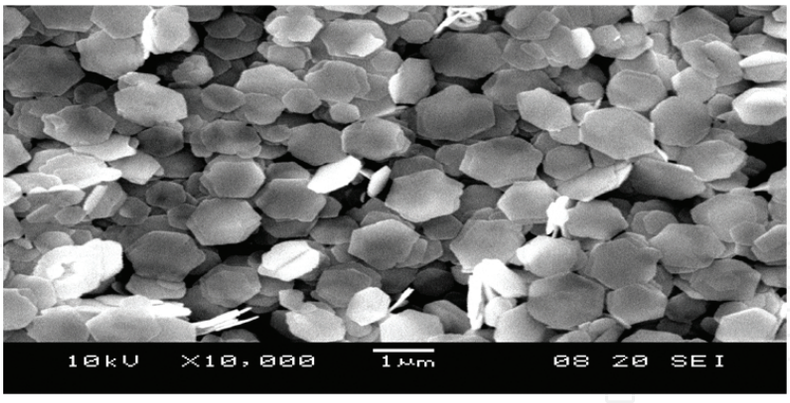

Figure 3. SEM image for PbMet-A sample as made.

The second example of a chemical compound prepared by LALE technique is the synthesis of II–VI semiconductor quantum dots (QDots). The reason for that interest seems to be the high technological potential that these materials present in several areas such as optic, electronic, catalyst application, solar photovoltaic cells, nanobar codes, field effect transistors, light emitting diodes and *in vivo* biomedical detection fluorescent tags in biology and the development of chemical and biological sensors [41–47]. Concerning to the CdS preparation, the

synthesis consists of the ablation of cadmium foil in the thiosulfate and thioglycerol solution for 5 minutes. As a consequence, a highly stable colloidal solution is obtained and presents a strong yellow fluorescence peak at 590 nm that can be seen by the naked eye when the sample is excited with UV light at 365 nm as shown in **Figure 4**.

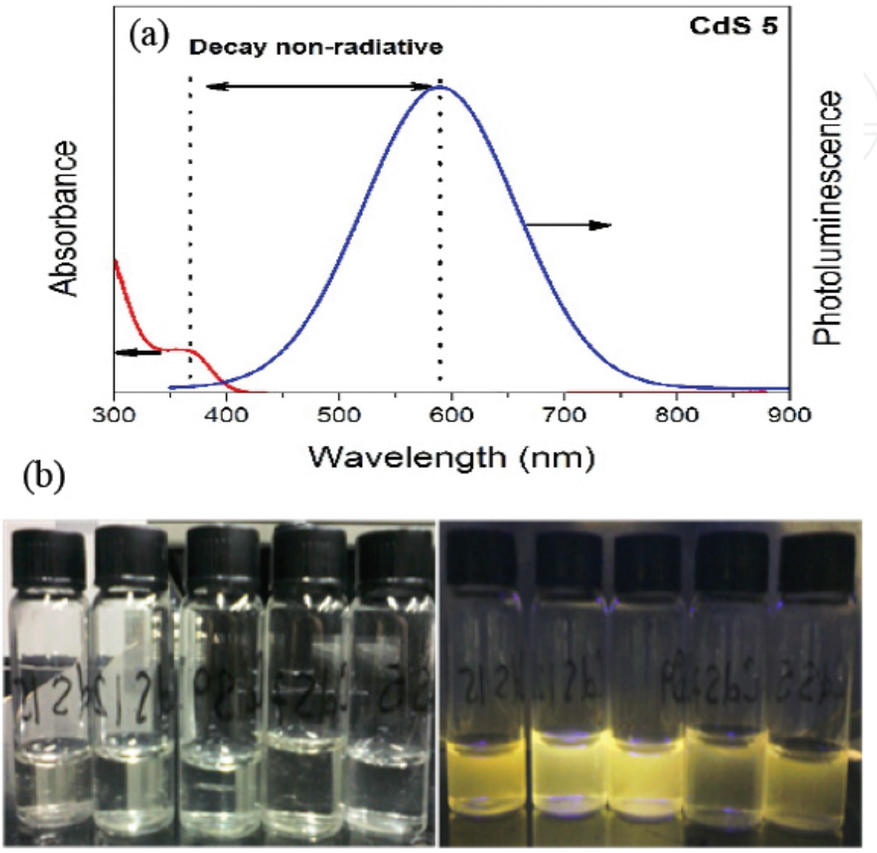

Figure 4. (a) The absorption luminescence spectra and (b) photograph of the CdS quantum dots solutions before and after excitation with UV lamp.

These results allow us to conclude that quantum confinement is observed since the absorption bands of the colloidal solution suffer a blue shift to 360 nm when compared with CdS bulk emission at 515 nm [47].

The mechanism proposed to explain the CdS quantum dots formation is shown in Eqs. (4)–(6), where the Cd target is ablated-producing ionizing species together with the action of thioglycerol as a catalyst for the thiosulfate hydrolysis [48, 49], which results *in situ* formation of sulfide ion (S^{2-}) and consequently the formation of CdS particle.

$$S_2O_3^{-2} + H_2O \xrightarrow{TG} SO_4^{-2} + H_2S \tag{4}$$

$$(m+n)Cd_{(s)} \xrightarrow{h\nu} nCd_{(s)} + mCd^{+2} + m2e \tag{5}$$

http://dx.doi.org/10.5772/66245

$$Cd^{+2} + S^{-2} \rightarrow CdS \tag{6}$$

Additionally, it can be seen that, in this process, thioglycerol is used as a hydrolyzing agent for thiosulfate (1) and as stabilizing agent for the nanoparticles.

From the analysis of the absorption spectra we found that the band gap of the CdS semiconductor is of the order of 3.1 eV and using the effective mass approximation method developed by Burs [50], we can estimate that the optical particle size is of the order of 3.2 nm. From the analysis of X-ray diffraction measurement of **Figure 5** and the comparison with the JCPDS card file number 10-454, we conclude that the CdS particle crystallize in a zinc blende structure and from the broadening of the diffraction peak we can see that the peaks present a very broad distribution indicating the presence of a very small crystallite size.

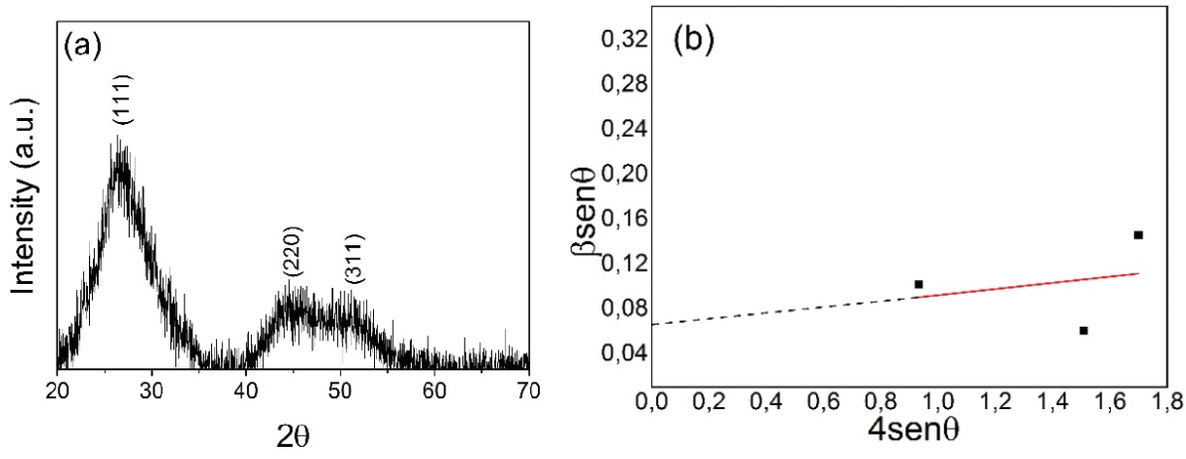

Figure 5. (a) X-ray diffraction of quantum dot CdS and (b) plot Willianson-Hall for crystallite size determination.

Using the Williamson-Hall method for the diffraction peaks analysis, we found that the crystallite size is of the order of 2.2 nm. This result is slightly smaller than those calculated by optics method. However, it indicates that we were successful in preparing very small CdS quantum dots particle. It is interesting to mention that the CdS nanocrystals possess the cubic space group, instead of the hexagonal wurtzite structure which is thermodynamically more stable. This probably could be attributed to the nonconventional chemical reaction condition of high pressures and temperatures which favors the occurrence of chemical processes in nonequilibrium conditions and the formation of materials with metastable configurations [51, 52].

The third example is the synthesis of magnetic iron samples. In this study, all prepared materials were dispersed or stabilized in liquid environment after synthesis. The samples were further characterized in a liquid phase by absorption spectroscopy in the ultraviolet and visible region. The materials of samples Type1, Type2 and Type3 were separated from the NaOH precursor solution by centrifugation and also washed in distilled water. A fraction of the prepared samples was precipitated on glass plates for the scanning electron microscopy

characterization, while another fraction of the samples was pulverized and subjected to X-ray diffraction, infrared spectroscopy and magnetic measurement. **Figure 6** shows UV-Vis spectra for the precursor solution of sodium hydroxide and for the resulting solutions of the preparation process for samples 1, 2 and 3.

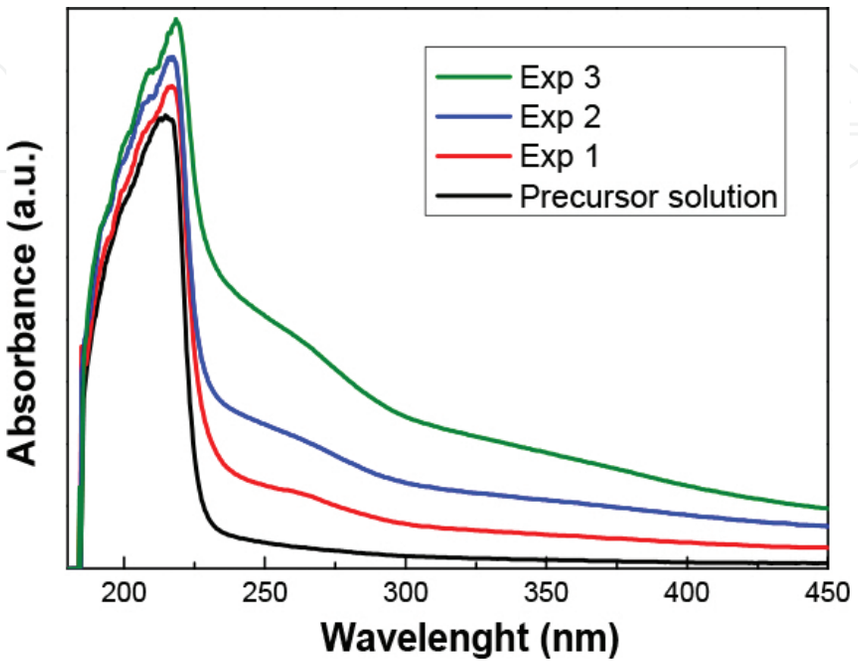

Figure 6. UV-Vis spectra of samples Type1, Type2 and Type3 and of precursor solution.

It is possible to see in **Figure 6** that the spectra of samples 1, 2 and 3 have three additional absorption bands when compared with the spectrum of the precursor solution of NaOH. These absorption bands are related to the presence of the dispersed material prepared in the solution resulting from laser ablation. It is also observed that the absorption bands were more intense for the materials prepared with the application of higher fluencies on the solid target. This fact indicates that the higher the fluency used in experiments, the higher is the amount of material obtained and dispersed in solution per unit time. This result is consistent with the UV-Vis spectrum for iron and iron oxide nanoparticles in aqueous solution. The absorption bands with maxima at 216 and 268 nm may be associated with iron nanoparticles, while the band located at 350 nm is likely due to other phases present in the samples [53].

From the analysis of the results obtained by ultraviolet and visible spectroscopy, FTIR, scanning electron microscopy, X-ray diffraction and magnetometry, it allowed us to conclude that all samples (named as Type1, Type2 and Type3) prepared, under three different experimental conditions, are nanostructured and formed respectively by: Type1 sample crystalline phases regarding the presence iron (Fe), iron oxide (FeO), sodium ferrate (V) ($NaFeO_3$), sodium ferrate (VI) (Na_2FeO_4) and sodium hydroxide (NaOH); Type2 sample, Fe, FeO, Na_2FeO_4 and NaOH; Type3 sample, Fe and FeO. The metastable FeO phase is especially interesting because it is generally prepared only at high temperatures and by rapid cooling process [51].

http://dx.doi.org/10.5772/66245

The prepared samples show magnetic properties, with the Fe and FeO (Type3) having the most intense magnetic response, whereas the Type1 sample shows intermediate intensity response and Type2 material shows the less intense magnetization response. Some modification of the synthesis conditions used in these experiments resulted in the preparation of ferrate sodium compound (V) ($NaFeO_3$) and sodium ferrate (VI) (Na_2FeO_4). In these compounds the iron atoms have a high oxidation number lying the state Fe^{+5} and Fe^{+6}. The FeO_3^{-1} and FeO_4^{-2} ferrate ions present high potential for technological application in several scientific areas, such as in the degradation of environmental pollutants and as disinfectants [54]. Furthermore, recent studies indicate that FeO_4^{-2} ions have promising applications as electrolytes materials in rechargeable batteries [55].

Thus, the laser ablation of iron targets in sodium hydroxide solution presents itself as a new method for the preparation of sodium ferrate, enabling control of the properties of materials prepared by tuning the fluency of laser pulses. To the best of our knowledge, obtaining sodium ferrate by ALAL and obtaining results regarding the control of crystallinity and magnetization of such samples by ALAL are unprecedented in the literature.

The scanning electron microscopy performed on samples Type1, Type2 and Type3 shows that these materials consist of particles of approximate spherical shape and with different size distribution for each type of material. **Figure 7(a)** shows the Type1 material consists of spherical particles with an average size of 170 nm that are both dispersed and isolated on the substrate or agglomerated as structures formed by larger particle clusters. **Figure 7(b)** shows that the Type2 material has particles with spherical shape and average size of the order of 0.7 μm and it seems that the distribution of particle sizes in this sample is wider than that presented by the sample Type1. **Figure 7(c)** shows that the SEM image is composed of agglomerated particles of 50 nm in size, where it is also possible to visualize a few micron size particles.

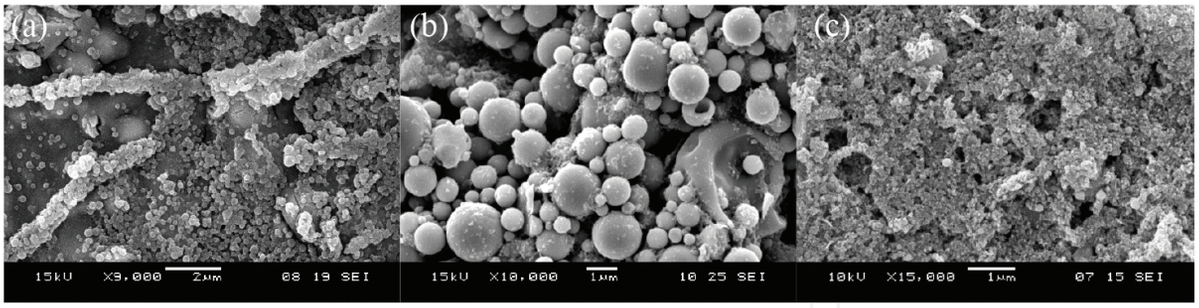

Figure 7. Image of SEM for: (a) Type1 sample; (b) Type2 sample; (c) Type3 sample.

The SEM shown in **Figure 7(a)–(c)** allowed to estimate the average size and average standard deviation for the size distribution of the particles in the samples Type1, Type2 and Type3. The results of these measurements are shown in **Table 2**.

These results indicate that the structural properties of the obtained materials are susceptible to the fluency of the laser beam used in the preparation procedure and therefore it is possible to control the size and size distribution of the sample by controlling the fluency. This behavior

may be related to the photolysis promoted by the laser beam onto the prepared particles and increases the ablated material density in the plasma plume. These two effects increase when the fluency is increased and their joint action could explain the observed results: photolysis tends to decrease the size of the particles while high density plume favors to obtain larger particles.

Sample	Average size	Standard deviation
1	170 nm	50 nm
2	0.7 μm	0.3 μm
3	50 nm	30 nm

Table 2. Estimate of the average size for Type1, Type2 and Type3 samples.

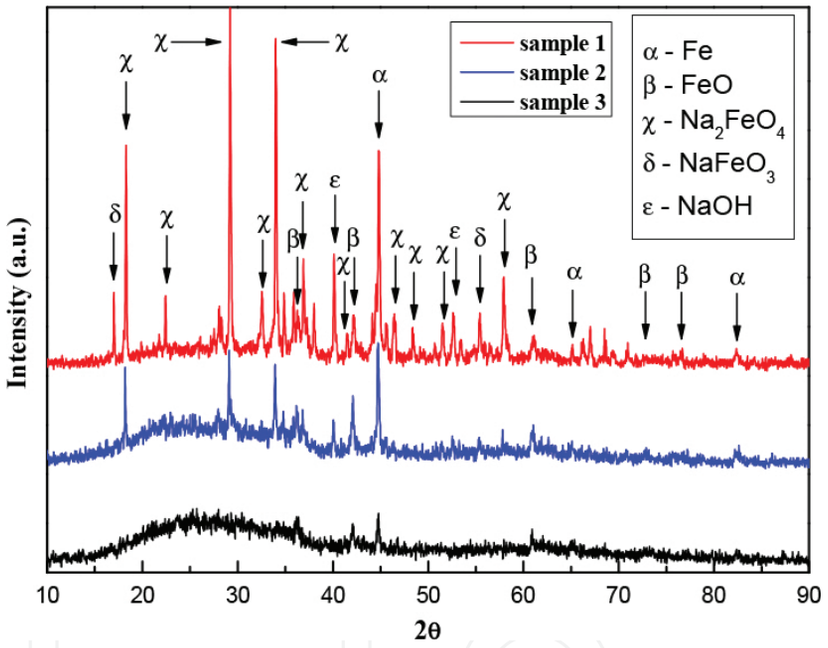

Figure 8. X-ray diffraction patterns of samples.

The X-ray diffraction was used for the identification and structural characterization of the prepared materials. The XRD patterns obtained for Type1, Type2 and Type3 samples are shown in **Figure 8**, where they are also indicating crystalline phases present in the samples that were identified by comparison with the software database PCPDF WIN of JCPDS-ICCD. Analyzing the XRD patterns of the samples and correlating the maximum diffracted intensity with the major peaks of diffraction patterns in JCPDS database is verified that prepared under Type1 experimental conditions is formed by crystalline phases regarding the presence of iron (Fe), iron oxide (FeO), sodium ferrate (V) ($NaFeO_3$), sodium ferrate (VI) (Na_2FeO_4) and sodium hydroxide (NaOH). The Type2 sample shows evidence of the presence of Fe, FeO, Na_2FeO_4,and NaOH, while in Type3 sample, the presence of Fe and FeO phases was only found. It is

http://dx.doi.org/10.5772/66245

interesting to notice that the FeO phase is metastable and can be prepared only at high temperatures and by a fast cooling process [51].

Figure 7 shows that when the fluency applied to the target solid surface increases, it is possible to observe progressively reducing on the crystallinity of the prepared samples. Clearly, the Type1 sample with a fluency of 0.5 J/cm^2 has well-defined crystalline phases, while Type3 sample prepared using 4.0 J/cm^2 fluency is majorly amorphous. This behavior can be explained by considering the rapid cooling effect of the liquid environment of the plasma plume. The temperature of the ablated material in the plume plasma should increase proportionally to the fluency of laser pulses; on the other hand, the cooling capacity of the liquid environment basically depends on the temperature and the volume of liquid used. In this way, the higher the fluency used, the higher the cooling rate due to liquid environment, because greater will be the temperature variation during the short time cooling.

The proposed cooling model can explain the crystalline dependence of the material obtained with the fluency of the laser beam used in the preparation process. The fluency values used during the preparation of the samples Type1, Type2 and Type3 correspond to cooling rates T_1, T_2 and T_3 and $T_3 > T_2 > T_1$. Although the specific time (time per mass) available for crystallization of the ablated material is higher in Type1 than in Type2, this in turn has the time available for crystallization higher than the Type3 sample. The short crystallization time for Type2 and Type3 samples inhibits the formation of well-defined crystalline phases, leaving the samples Type2 and Type3 less crystalline and substantially amorphous.

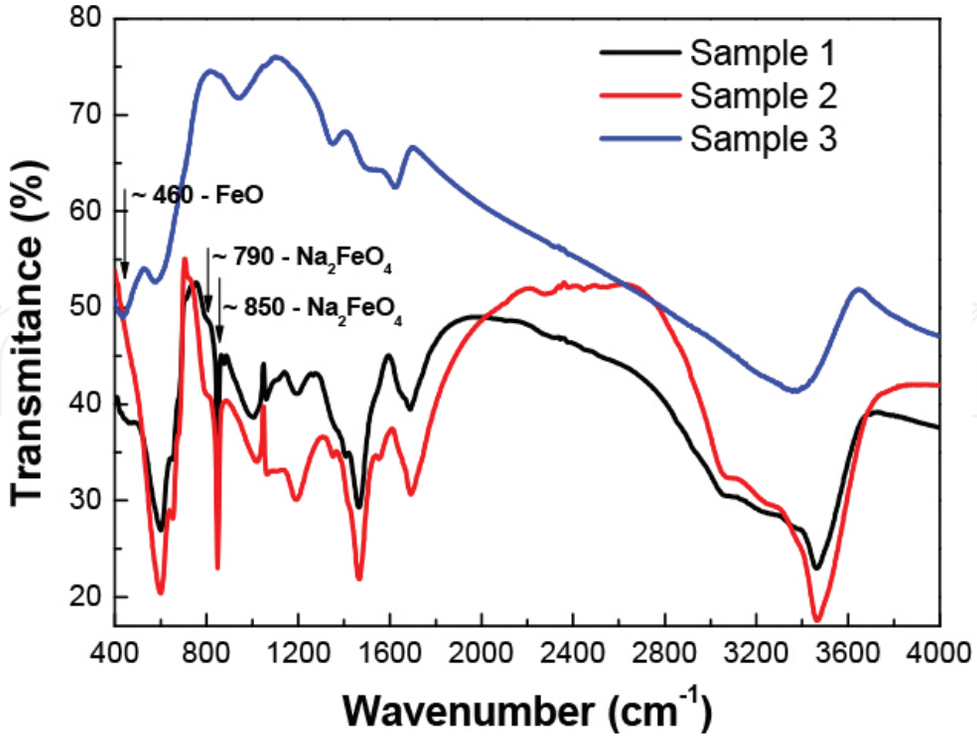

Figure 9. IR transmittance spectrum.

Figure 9 shows the infrared transmission spectra (IR spectra) for the materials prepared. It is observed that most of the absorption modes of Type1 and Type2 materials coincide, although it does not happen for sample Type3. This indicates that the composition and chemical structure of Type1 and Type2 samples are similar, while they differ from the composition and structure presented by the sample Type3. Comparing the IR spectra obtained from data available in [56] literature it was possible to verify the presence of Na_2FeO_4 in Type1 and Type2 samples by identifying active stretching and vibration modes relating to the tetrahedral distribution of four oxygens around the Fe ion (VI). The modes for the Na_2FeO_4 are not displayed in the IR spectrum of Type3 sample confirming the assumption that Type1 and Type2 samples are chemically similar and that the composition of the sample differs from that presented by Type3. The presence of FeO in all samples was attributed comparing it with data from the literature [57]. The IR spectroscopic analysis results corroborate the X-ray diffraction.

Figure 10 shows the magnetization curves measured as a function of applied magnetic field for the samples Type1, Type2 and Type3. The analysis of magnetization curves indicates that all samples exhibit hysteresis, thus being classified as ferromagnetic, although it is noticed that the magnetic response is different for each sample. When the materials are subjected to a field of the same intensity, Type3 material has higher magnetization, this value is higher than the Type1 and Type2 samples and the Type2 sample has the lowest value of magnetization.

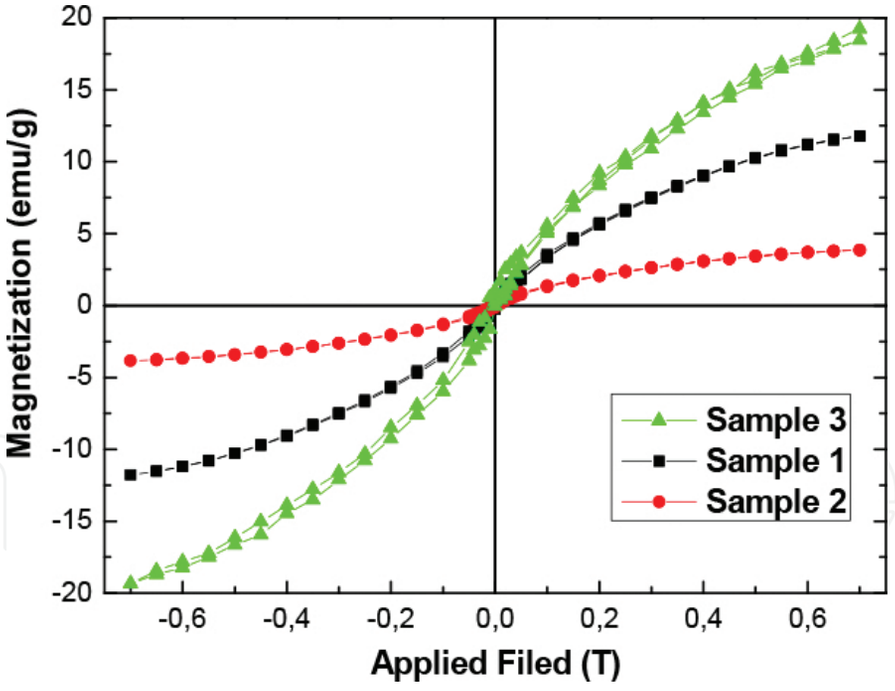

Figure 10. Magnetization per unit mass as a function of applied magnetic field.

The magnetic response of samples can be related to the size of their structures. It was observed in this experiment that for the same value of applied magnetic field, the magnetization of the module M (H) of Type1, Type2 and Type3 samples increases with decreasing diameter, D, of the particles in the sample. In other words, it was found that $M(H)_{Type3} > M(H)_{Type1} > M(H)_{Type2}$

http://dx.doi.org/10.5772/66245

while $D_{Type3} > D_{Type1} > D_{Type2}$. We observed size effects on the magnetic response of the samples, possibly related to the size and presence of magnetic monodomain within the particles of a smaller size, while larger particles should contain several oriented monodomain randomly causing a less effective magnetic response.

We can also qualitatively relate the magnetic behavior of the samples to their chemical composition: The Type1 sample is formed by phases Fe, FeO, $NaFeO_3$, Na_2FeO_4,and NaOH, while Type2 sample is formed by Fe, FeO, Na_2FeO_4,and NaOH and Type3 by Fe and FeO. It is known that unpaired electrons in the atomic orbitals of a material are responsible for their magnetic properties and the greater the number of unpaired electrons will be, the higher its magnetization per unit mass. Iron atoms in Fe and FeO phases are respectively 4 and 4 unpaired electrons. However, the phase $NaFeO_3$ the iron atoms present only 3 unpaired electrons and Na_2FeO_4 phase 2 has unpaired electrons. Since the magnetization was measured by mass, this argument justified the reason that Type3 sample, composed of Fe and FeO, is the most intense magnetic response. The Type1 material its intermediate intensity response and the Type2 material is the less intense magnetization ($M(H)_{Type3} > M(H)_{Type1} > M(H)_{Type2}$).

We can summarize that the preparation of micro- and nanostructured magnetic particles through ALAL iron targets of sodium hydroxide 1 M was successfully obtained. The results demonstrate that structural and magnetic properties of the materials prepared are influenced by the applied laser beam fluency during the ablation process. Specifically it was found that the fluency can be used to control the size distribution of structures present in the sample as well as controlling the magnetization and the crystallinity of the material prepared.

The fourth and fifth examples are the synthesis of the MOFs and LMOFS. For the synthesis of metal organic framework, we have developed two procedures: for the $Cu_3(BTC)_2(H_2O)_3$ preparation, a cupper metal powder was used as a target, while for the synthesis of the luminescent MOF $Eu(TMA)(H_2O)_4$, a metal oxide powder was used as a target instead.

We chose the metal organic frameworks (MOFs) materials as the next example for the fact that this structure are quite complex and consist of a three-dimensional (3D) metal coordination network formed by metal ions or clusters linked together by organic bridging ligands. Consequently, this material presents high surface area, uniform small porous architecture [58], open metal sites [59], possibility of structure modification through postsynthesis functionalization routes [60], that together with luminescent proprieties make MOFs materials promising for several applications such as gas storage, gas separation, heterogeneous catalysis [61, 62], sensing devices [63, 64], ion exchange [65, 66], optoelectronics [67, 68] and efficient phosphors for displays and lighting [69]. Regarding to the sample preparation, almost all methods used for MOFs preparation are time consuming, except for the microwave-assisted processes and therefore new methods should be developed in order to overcome this advantage.

The main difference between the methods applied before for the materials preparation is the fact that for the $Cu_2(BTC)_2(H_2O)_3$ preparation, Cupper metal powder dispersed in liquid medium was used as a target, whereas to synthesize $Eu(BTC)(H_2O)_4$, europium oxide was used as a target. In both syntheses, magnetic stirring was used to homogenize the suspension in a

solution of trimesic acid dissolved in water and DMF. In $Cu_2(BTC)_2(H_2O)_3$ case, $NaNO_3$ was also used as oxidizing agent.

To explain the formation of $Cu_2(BTC)_2(H_2O)_3$, the mechanism proposed consists of a combination of two simultaneous processes. The first step involves the ablation of the metal surface, producing the ejection of the plume containing Cu^0 and metal ion Cu^{+1} and Cu^{+2} and also the photochemical decomposition of nitrate ions, that results in hydroxyl radicals (•OH) production, which in turn results in the increase of the amount of Cu^{+2}. Finally, the Cu^{+2} reacts with the BTC to form the $Cu_3(BTC)_2.(H_2O)_2$ framework, as shown in Eq. (7)–(12).

$$Cu^0_{(s)} + h\upsilon \xrightarrow{HDMF^+\ BTC^{3-}\ NO_3^-} Cu^0_{(plasma)} + Cu^{1+}_{(plasma)} + Cu^{2+}_{(plasma)} \tag{7}$$

$$NO^-_{3(aq)} + h\upsilon \xrightarrow{HDMF^+\ BTC^{3-}\ NO_3^-} NO_{(g)} + O^-_{2(aq)} \tag{8}$$

$$O^-_{2(aq)} + 2H_2O_{(l)} \xrightarrow{HDMF^+\ BTC^{3-}\ NO_3^-} 2OH^o + 2H_2O_{(l)} \tag{9}$$

$$2OH^o \xrightarrow{DMF\ BTC^{3-}\ NO_3^-} H_2O_{(l)} + [O] \tag{10}$$

$$Cu^0_{(plasma)} + [O] \xrightarrow{DMF\ BTC^{3-}\ NO_3^-} 3Cu^{2+}_{(aq)} + H_2O_{(l)} \tag{11}$$

$$3Cu^{2+}_{(aq)} + 2BTC^{3-} \xrightarrow{DMF\ O_3^-} Cu_3(BTC)_2(H_2O)_3 + 4H_2O_{(l)} \tag{12}$$

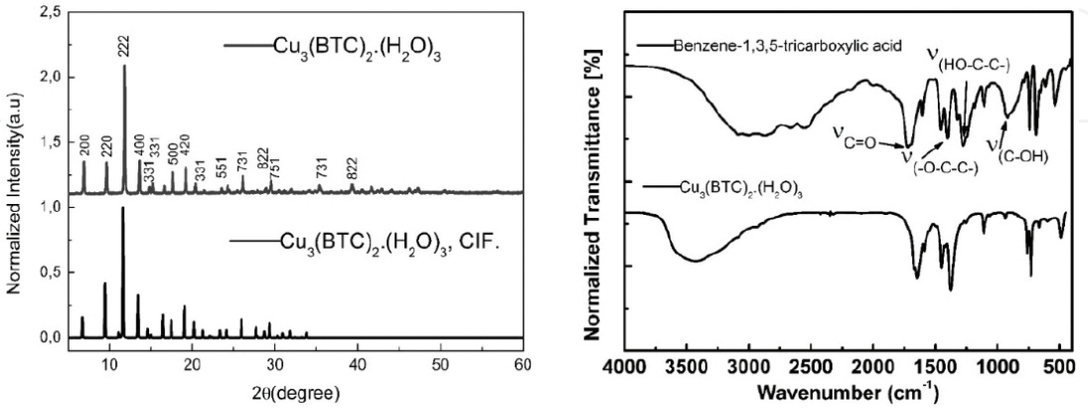

Figure 11. X-ray diffraction patterns (left) and FT–IR analysis (right) of $[Cu_3(BTC)_2]$-MOF prepared by laser ablation techniques at room temperature.

http://dx.doi.org/10.5772/66245

Figures 11 and **12** show the results of X-ray diffraction, infrared and scanning electron microscopy, which confirm that $Cu_2(BTC)_2(H_2O)_3$ MOFs has been successively prepared [20].

For the $Eu(BTC)(H_2O)_6$ preparation, it is noticed that the ablation of europium oxide (Eu_2O_3) make available Eu^{3+} ions in solution, which reacts with BTC molecules to form a luminescent network as shown in **Figure 13**. **Figure 14** shows the structural and spectroscopic characterization of the obtained compound, thus from the X-ray diffraction results we can conclude that the obtained LMOFs presents highly crystallinity with diffraction peaks isomorphic with $Eu(BTC)(H_2O)_6$. The FTIR analysis shows the disappearance of the carboxyl group in 1721 cm^{-1} and the appearance of the modes in 1404 and 1275 cm^{-1}, strongly suggesting that the Eu^{3+} ion is coordinated with the carbonyl group. Finally, the emission analysis shows that the compound exhibits an intense luminescence in the red region of the visible spectra λ = 611 nm, characteristic $^5D_0$-$^7F_2$ transition of Eu^{3+} ions when irradiated with UV light at λ = 254 nm, with a quantum efficiency of 10.8% and life time of 0.26 ms.

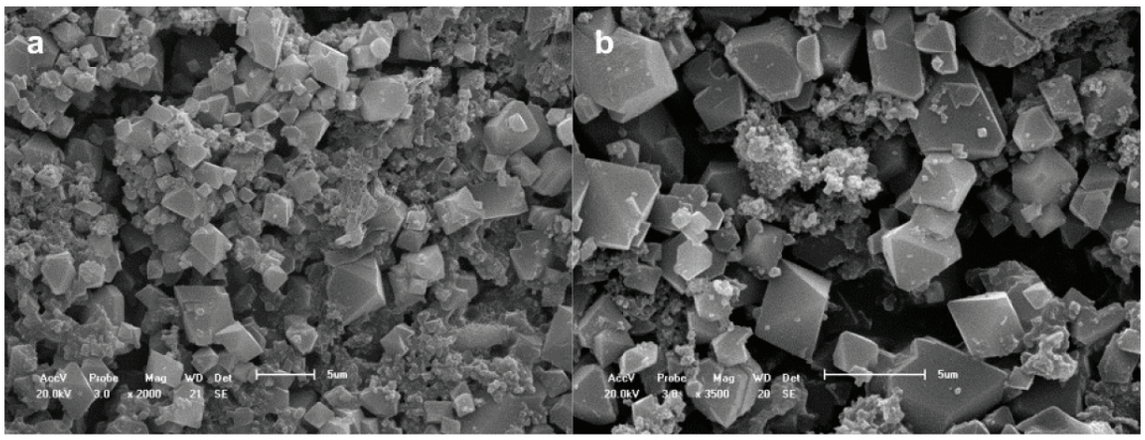

Figure 12. Morphologic analysis of $Cu_3(BTC)_2(H_2O)$ crystals prepared by the laser ablation technique as a function of the ablation time for: (a) 60 min, (b) 90 min.

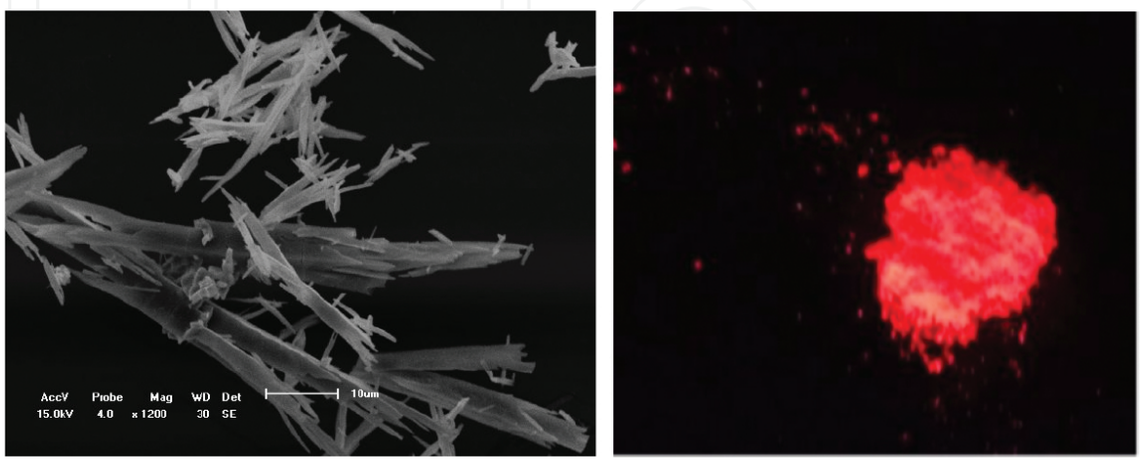

Figure 13. SEM image of $Eu(TMA)(H_2O)_4$ and a photograph under UV excitation λ = 254 nm.

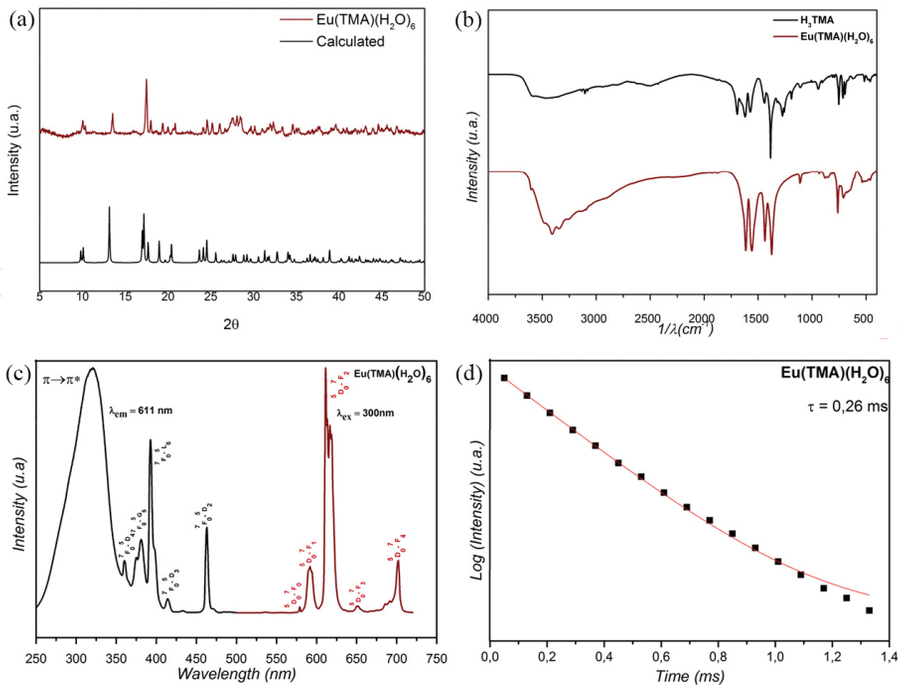

Figure 14. Structural and spectroscopic characterization: (a) XRD patterns of $Eu(BTC)(H_2O)_6$; (b) FT-IR spectrum of H_3TMA and $Eu(TMA)(H_2O)_6$; (c) photoluminescence and excitation spectra of $Eu(BTC)(H_2O)_6$ at room temperature; (d) luminescence decay curves at room temperature of the emitting $^5D_0$ level of the Eu^{3+} in $Eu(BTC)(H_2O)_6$.

From the results above, we conclude that we have succeeded in synthesizing a three-dimensional networks $Eu(TMA)(H_2O)_6$ and $Cu_3(BTC)_2.(H_2O)_2$ producing, for the first time, a metal-organic framework by laser ablation in liquid, wherein both obtained materials were crystalline and with well-defined morphology. Comparing with the conventional method, it is observed that this new synthesis route has the advantage of being a one-step synthesis, which allows obtaining submicromaterial with a high yield [21].

5. Conclusions

We have successfully developed a new technique for the synthesis of micro- and nanostructured materials using laser ablation in liquid environment, which consists of the combination of the target ablation in a liquid environment together with the photo physical or chemical decomposition of the solvent. With these method, several compounds, such as $Cu_2(BTC)_2(H_2O)_3$, $Eu(TMA)(H_2O)_4$, CdS quantum dots and magnetic materials such as Fe, FeO, $NaFeO_3$, Na_2FeO_4 have been prepared.

For each material prepared above, we observed that there was a different set of synthesis parameter to be adjusted in order to obtain the desired material. However, when compared with the conventional methods of synthesis, we can see that laser ablation in liquid is a straightforward technique with few adjustable parameter that allowed materials to be prepared with a high yield. As a matter of fact, with these examples we feel confident to propose this technique as the next-generation tool for the materials preparation.

http://dx.doi.org/10.5772/66245

Acknowledgements

This work was supported by Conselho Nacional de Desenvolvimento Cientifico e Tecnologico (CNPq) contract number 308008/2013-8, Coordenacao de Aperfeicoamento de Pessoal de Nivel Superior (CAPES), Fundacao de Amparo a Ciencia e Tecnologia do Estado de Pernambuco (FACEPE) and Programa de Recursos Humanos da ANP para o Setor Petróleo e Gás – PRH-ANP/MCTI. We also would like to thank Núcleo de Dispositivos Ópticos, Eletrônicos e Magnéticos (NUDOM), from NICIT-CAA and to Ms. Moralinda for grammar review.

Author details

Walter Mendes de Azevedo[1*], Sérgio de Lemos Campello[2*], Diego Leite da Cunha[3], Leonardo Tadeu Boaes de Mendonça[1] and Ohanna Maria Menezes Madeiro da Costa[4]

*Address all correspondence to: wma@ufpe.br and slcampello@yahoo.com.br

1 Department of Fundamental Chemistry, Federal University of Pernambuco, Recife, PE, Brazil

2 Interdisciplinary Nucleus of Exact Science and Technological Innovation, Federal University of Pernambuco, Recife, PE, Brazil

3 Faculdade Boa Viagem/DeVry Brasil, Recife, PE, Brazil

4 Postgraduate Program in Materials Science, Federal University of Pernambuco, Recife, PE, Brazil

References

[1] Srinivasan, R. and B. Braren, *Ultraviolet laser ablation of organic polymers*. Chemical Reviews, 1989. 89(6): pp. 1303–1316.

[2] Lazare, S. and V. Granier, *Ultraviolet laser photoablation of polymers: a review and recent results*. Laser Chemistry, 1989. 10(1): pp. 25–40.

[3] Bäuerle, D.W., *Laser processing and chemistry*. 2011: Springer-Verlag Berlin Heidelberg.

[4] Leon J. Radziemski, D.A.C., *Laser-induced plasma and applications*. 1989: CRC Press, New York.

[5] John C. Miller, R.F.H.J., *Laser ablation mechanisms and applications*. 1991: Springer New York, New York.

[6] Fogarassy, E. and S. Lazare, *Laser ablation of electronic materials: basic mechanisms and applications*. European Materials Research Society monographs. 1992, Amsterdam; New York: North-Holland. xi, 394 p.

[7] Chrisey D.B., Hubler G.K., Pulsed laser deposition of thin solid films. 1994: Wiley-Interscience, New York. 648.

[8] Yang, G.W., *Laser ablation in liquids: Applications in the synthesis of nanocrystals*. Progress in Materials Science, 2007. 52(4): pp. 648–698.

[9] Zeng, H., et al., *Nanomaterials via Laser Ablation/Irradiation in Liquid: A Review*. Advanced Functional Materials, 2012. 22(7): pp. 1333–1353.

[10] Furusawa, H., T. Sakka and Y.H. Ogata, *Characterization of ablated species in laser-induced plasma plume*. Journal of Applied Physics, 2004. 96(2): pp. 975–982.

[11] Mafuné, F., et al., *Full physical preparation of size-selected gold nanoparticles in solution: laser ablation and laser-induced size control*. The Journal of Physical Chemistry B, 2002. 106(31): pp. 7575–7577.

[12] Mafuné, F., et al., *Formation of stable platinum nanoparticles by laser ablation in water*. The Journal of Physical Chemistry B, 2003. 107(18): pp. 4218–4223.

[13] Mafuné, F., et al., *Structure and stability of silver nanoparticles in aqueous solution produced by laser ablation*. The Journal of Physical Chemistry B, 2000. 104(35): pp. 8333–8337.

[14] Mafuné, F., et al., *Formation and size control of silver nanoparticles by laser ablation in aqueous solution*. The Journal of Physical Chemistry B, 2000. 104(39): pp. 9111–9117.

[15] Pyatenko, A., et al., *Synthesis of silver nanoparticles by laser ablation in pure water*. Applied Physics A, 2004. 79(4-6): pp. 803–806.

[16] Takeuchi, Y., T. Ida and K. Kimura, *Colloidal stability of gold nanoparticles in 2-propanol under laser irradiation*. The Journal of Physical Chemistry B, 1997. 101(8): pp. 1322–1327.

[17] Sylvestre, J.-P., et al., *Stabilization and size control of gold nanoparticles during laser ablation in aqueous cyclodextrins*. Journal of the American Chemical Society, 2004. 126(23): pp. 7176–7177.

[18] da Cunha, D.L., et al., *Nanostructured hydrocerussite compound (Pb3(CO3)2(OH)2) prepared by laser ablation technique in liquid environment*. Materials Research Bulletin, 49(0): pp. 172–175.

[19] Mendonça, L.T.B. and W.M. de Azevedo, *A fast bottom-up route for preparing CdS quantum dots using laser ablation in a liquid environment*. Journal of Luminescence, 2016. 171: pp. 79–84.

[20] Campello, S.L., et al., *Laser ablation: A new technique for the preparation of metal-organic frameworks Cu3(BTC)2(H2O)3*. Materials Letters, 2015. 148: pp. 200–203.

[21] da Costa, O.M.M.M. and W.M. de Azevedo, *Highly luminescent metal organic framework Eu(TMA)(H_2O)$_4$ materials prepared by laser ablation technique in liquid*. Journal of Luminescence, 2016. 170, Part 2: pp. 648–653.

[22] Ma, R., et al., *Synthesis and fluorescence properties of ten lanthanide benzene-1,3,5-tricarboxylate complexes*. Spectrochimica Acta Part A: Molecular and Biomolecular Spectroscopy, 2010. 77(2): pp. 419–423.

[23] Souza, E.R., *Síntese de complexos benzenotricarboxilatos de terras raras e estudo de suas propriedades fotoluminescentes*, in *Instituto de Química*. 2008, Universidade de São Paulo: São Paulo.

[24] Martinetto, P., et al., *Synthetic hydrocerussite, 2PbCO3.Pb(OH)2, by X-ray powder diffraction*. Acta Crystallographica Section C, 2002. 58(6): pp. i82–i84.

[25] Welcomme, E., et al., *Investigation of white pigments used as make-up during the Greco-Roman period*. Applied Physics A, 2006. 83(4): pp. 551–556.

[26] Walter, P., et al., *Making make-up in Ancient Egypt*. Nature, 1999. 397(6719): pp. 483–484.

[27] Rachel Billinge, L.C., J. Dunkerton, S. Foister, J. Kirby, J. Pilc, A. Roy, M. Spring and R. White, Methods and materials of northern european painting in the national gallery, 1400–1550. National Gallery Technical Bulletin, 1997. 18, 6–55.

[28] Krivovichev, S.V. and P.C. Burns, *Crystal chemistry of basic lead carbonates. I. Crystal structure of synthetic shannonite, $Pb_2O(CO_3)$*. Mineralogical Magazine, 2000. 64(6): pp. 1063–1068.

[29] Frost, R.L., et al., *Raman spectroscopy of selected lead minerals of environmental significance*. Spectrochimica Acta Part A: Molecular and Biomolecular Spectroscopy, 2003. 59(12): pp. 2705–2711.

[30] Michell, E.W.J. and K.Y. Ng, *X-Ray powder diffraction studies of hydrocerussite (basic lead carbonate) as a stabiliser in plasticised polyvinyl chloride*. British Polymer Journal, 1980. 12(3): pp. 114–120.

[31] Steele, I.M.P., J. Joseph and A. Livingstone, *Crystal structure of susannite, Pb4SO4(CO3)2(OH)2: a trimorph with macphersonite and leadhillite*. European Journal of Mineralogy, 1999. 11(3): pp. 493–499.

[32] Porter, R.P. and W.A. Noyes, *Photochemical Studies. LIV. Methanol Vapor1*. Journal of the American Chemical Society, 1959. 81(10): pp. 2307–2311.

[33] Sakong, S. and A. Gross, *Total oxidation of methanol on Cu(110): a density functional theory study*. The Journal of Physical Chemistry A, 2007. 111(36): pp. 8814–8822.

[34] Walling, C. and R.W.R. Humphreys, *Photooxidation of alcohols by ferric ion*. The Journal of Organic Chemistry, 1981. 46(7): pp. 1260–1263.

[35] Fievet, F., et al., *Homogeneous and heterogeneous nucleations in the polyol process for the preparation of micron and submicron size metal particles*. Solid State Ionics, 1989. 32: pp. 198–205.

[36] Ducamp-Sanguesa, C., R. Herrera-Urbina and M. Figlarz, *Synthesis and characterization of fine and monodisperse silver particles of uniform shape*. Journal of Solid State Chemistry, 1992. 100(2): pp. 272–280.

[37] Fievet, F., et al., *Controlled nucleation and growth of micrometre-size copper particles prepared by the polyol process*. Journal of Materials Chemistry, 1993. 3(6): pp. 627–632.

[38] Ducamp-Sanguesa, C., R. Herrera-Urbina and M. Figlarz, *Fine palladium powders of uniform particle size and shape produced in ethylene glycol*. Solid State Ionics, 1993. 63: pp. 25–30.

[39] de Azevedo, W.M. and F.D. Menezes, *A new and straightforward synthesis route for preparing Cds quantum Dots*. Journal of Luminescence, 2012. 132(7): pp. 1740–1743.

[40] Bucca, M., et al., *Nucleation and crystallization of otavite, witherite, calcite, strontianite, hydrozincite and hydrocerussite by CO_2 membrane diffusion technique*. Chemical Geology, 2009. 266(3–4): pp. 143–156.

[41] Steigerwald, M.L. and L.E. Brus, *Semiconductor crystallites: a class of large molecules*. Accounts of Chemical Research, 1990. 23(6): pp. 183–188.

[42] Bawendi, M.G., M.L. Steigerwald and L.E. Brus, *The quantum mechanics of larger semiconductor clusters ("Quantum Dots")*. Annual Review of Physical Chemistry, 1990. 41(1): pp. 477–496.

[43] Alivisatos, A.P., *Semiconductor Clusters, Nanocrystals and Quantum Dots*. Science, 1996. 271(5251): pp. 933–937.

[44] Colvin, V.L., M.C. Schlamp and A.P. Alivisatos, *Light-emitting diodes made from cadmium selenide nanocrystals and a semiconducting polymer*. Nature, 1994. 370(6488): pp. 354–357.

[45] Klein, D.L., et al., *A single-electron transistor made from a cadmium selenide nanocrystal*. Nature, 1997. 389(6652): pp. 699–701.

[46] Bruchez, M., et al., *Semiconductor nanocrystals as fluorescent biological labels*. Science, 1998. 281(5385): pp. 2013–2016.

[47] Mandal, P., et al., *Orange-red luminescence from Cu doped CdS nanophosphor prepared using mixed Langmuir–Blodgett multilayers*. The Journal of Chemical Physics, 2008. 128(11): p. 114703.

[48] Unni, C., D. Philip and K.G. Gopchandran, *Studies on optical absorption and photoluminescence of thioglycerol-stabilized CdS quantum dots*. Spectrochimica Acta Part A: Molecular and Biomolecular Spectroscopy, 2008. 71(4): pp. 1402–1407.

[49] Unni, C., et al., *Aqueous synthesis and characterization of CdS, CdS:Zn2+ and CdS:Cu2+ quantum dots*. Spectrochimica Acta Part A: Molecular and Biomolecular Spectroscopy, 2009. 72(4): pp. 827–832.

[50] Brus, L., *Electronic wave functions in semiconductor clusters: experiment and theory*. The Journal of Physical Chemistry, 1986. 90(12): pp. 2555–2560.

[51] Patil, P., et al., *Pulsed-laser-induced reactive quenching at liquid-solid interface: Aqueous oxidation of iron*. Physical review letters, 1987. 58(3): pp. 238–241.

[52] Yang, G.-W., J.-B. Wang and Q.-X. Liu, *Preparation of nano-crystalline diamonds using pulsed laser induced reactive quenching*. Journal of Physics: Condensed Matter, 1998. 10(35): p. 7923.

[53] Alqudami, A. and S. Annapoorni, *Fluorescence from metallic silver and iron nanoparticles prepared by exploding wire technique*. Plasmonics, 2007. 2(1): pp. 5–13.

[54] Sharma, V.K., et al., *Ferrates (iron(VI) and iron(V)): environmentally friendly oxidants and disinfectants*. Journal of Water and Health, 2005. 3(1): pp. 45–58.

[55] Koltypin, M., et al., *The study of K2FeO4 (Fe6+-super iron compound) as a cathode material for rechargeable lithium batteries*. Journal of Power Sources, 2005. 146(1–2): pp. 723–726.

[56] He, W., et al., *Electrochemical preparation, characterization and discharge performance of solid K[3]Na(FeO[4])[2]*. Vol. 9. 2007, Amsterdam, PAYS-BAS: Elsevier. 4.

[57] Ni, Y., et al., *Synthesis and characterization of α-FeO(OH) nano-rods in situ via a solution-oxidation*. Materials Letters, 2001. 49(3–4): pp. 185–188.

[58] Ferey, G., *Hybrid porous solids: past, present, future*. Chemical Society Reviews, 2008. 37(1): pp. 191–214.

[59] Britt, D., et al., *Highly efficient separation of carbon dioxide by a metal-organic framework replete with open metal sites*. Proceedings of the National Academy of Sciences, 2009. 106(49): pp. 20637–20640.

[60] Kitaura, R., et al., *A pillared-layer coordination polymer network displaying hysteretic sorption: [Cu2(pzdc)2(dpyg)]n (pzdc= Pyrazine-2,3-dicarboxylate; dpyg=1,2-Di(4-pyridyl)glycol)*. Angewandte Chemie International Edition, 2002. 41(1): pp. 133–135.

[61] Min Wang, Q., et al., *Metallo-organic molecular sieve for gas separation and purification*. Microporous and Mesoporous Materials, 2002. 55(2): pp. 217–230.

[62] Alaerts, L., et al., *Probing the lewis acidity and catalytic activity of the metal–organic framework [Cu3(btc)2] (BTC=Benzene-1,3,5-tricarboxylate)*. Chemistry – A European Journal, 2006. 12(28): pp. 7353–7363.

[63] Liu, L., et al., *Ionothermal synthesis of the Metal-Organic Framework compound Cu3(BTC)2*, in *Studies in Surface Science and Catalysis*. 2008, Elsevier. pp. 459–462.

[64] Himeur, F., et al., *The ionothermal synthesis of metal organic frameworks, Ln(C9O6H3)((CH3NH)2CO)2, using deep eutectic solvents*. Solid State Sciences. 12(4): pp. 418–421.

[65] Liao, J.-H., P.-C. Wu and Y.-H. Bai, *Eutectic mixture of choline chloride/urea as a green solvent in synthesis of a coordination polymer: [Zn(O3PCH2CO2)] Â · NH4*. Inorganic Chemistry Communications, 2005. 8(4): pp. 390–392.

[66] Zhang, J., et al., *Versatile structure-directing roles of deep-eutectic solvents and their implication in the generation of porosity and open metal sites for gas storage*. Angewandte Chemie International Edition, 2009. 48(19): pp. 3486–3490.

[67] Parnham, E.R., et al., *Ionothermal materials synthesis using unstable deep-eutectic solvents as template-delivery agents*. Angewandte Chemie, 2006. 118(30): pp. 5084–5088.

[68] Kuang, D., T. Brezesinski and B. Smarsly, *Hierarchical porous silica materials with a trimodal pore system using surfactant templates*. Journal of the American Chemical Society, 2004. 126(34): pp. 10534–10535.

[69] Rodrigues, M.O., et al., *Tb3+→Eu3+ energy transfer in mixed-lanthanide-organic frameworks*. The Journal of Physical Chemistry C, 2012. 116(37): pp. 19951–19957.